MINERALOGICAL MAGAZINE, JUNE 1976, VOL. 40, PP. 565–77

A metallographic and petrological study of metal–silicate fragments in the >1 mm size range from lunar soil 14162,80.

S. O. AGRELL,[1] H. J. AXON,[2] AND J. I. GOLDSTEIN[3]

SUMMARY. Optical and microprobe investigations have been made on the metal and silicate portions of four particles > 1 mm extracted from the magnetic fraction of lunar soil bulk sample 14162,80. Three of the particles have structures and compositions similar to those encountered in the < 1-mm fraction of this bulk sample. One of the particles shows a complex arrangement of melted metal, unmelted metal, micronorite, and vitroclastic silicate material. The structure of this particle is reported in detail and its structure is explained in terms of preferential melting of metal–phosphide interfaces under the influence of shock events operating on material at a temperature of about 650 °C.

ON earth it is unusual to find metallic iron of natural origin. Terrestrial native iron is encountered under very exceptional circumstances as in the Disco lava flows, but a more extensive range of extraterrestrial, meteoritic, iron-nickel material has been catalogued by Hey (1966). Meteoritic metal is encountered on earth as individual samples ranging from less than centimetre up to metre dimensions but its occurrence is severely localized.

On the moon, by contrast, metallic iron and iron-nickel alloy is found as an ubiquitous minor ($\sim\frac{1}{2}$ wt. %) component of all lunar soils although the individual metallic particles are usually less than $\frac{1}{2}$ mm long. Metallic particles of similar size are encountered in lunar basalts and lunar breccia rocks. The metal in lunar igneous rocks may well be native to the moon but Goldstein *et al.* (1972) (1973) have argued that at least some of the metal of the breccia rocks had its origin in meteoritic projectiles. The moon has no atmosphere to retard the projectiles, which are consequently damaged and dispersed in crater-forming impacts. By contrast, most projectiles that encounter the earth are either totally consumed by atmospheric ablation or are retarded to such an extent that they make a soft landing. However, occasionally, when a giant projectile does penetrate the earth's atmosphere with sufficient energy to form a 'lunar' type explosion crater some of the meteoritic projectile is converted into forms analogous to those encountered on the moon. For example, metallic droplets of 10 to 100 μm size emplaced in shock-altered country rock and remelted metal–sulphide–phosphide spheroids of about millimetre size scattered on the soil surrounding the Barringer meteorite crater in Arizona have been studied separately by Brett (1965) and by Blau *et al.* (1973) and have been compared by Kelly *et al.* (1974).

[1] University of Cambridge. [2] University of Manchester.
[3] Lehigh University, Pennsylvania 18015.

The present authors J. I. G. and H. J. A. have previously paid most attention to metal particles in the size range 100 to 500 μm that were extracted from the <1-mm sieve fraction of lunar soils. No massive metal fragments equivalent to the Cañon Diablo rim samples from the Barringer crater have been reported from the moon but to complete our investigations of Apollo 14 soils it appeared worth while to search for and examine the largest metal fragments in the >1-mm soil fraction, to see if there were any fragments of meteoritic debris that might have escaped alteration in the lunar environment.

This paper describes the structure of four of the largest metallic particles that have been recovered from Apollo 14 soil to date and a discussion of the thermal history and origin of these particles is attempted.

TABLE I. *Microprobe compositions, sizes, and microstructures of metal particles from Apollo 14 soil 14162,80*

Designation of particle	Size mm max dimension	Composition weight %				Structure
		Ni	Co	P	S	
3	2	5·4	0·36	0·17	—	Polycrystal α+Neumann bands
4	1·3	6·1	0·55	0·08	—	α_2, recrystallized α, minor Neumann bands
5	2·6	6·45	0·29	0·24	<0·02	Recrystallized α
		6·6	0·27	0·29	0·75	α+FeS
		6·5	0·25	0·30	0·63	Metallic droplets in glass
7	2	3·92	0·25	0·51	<0·02	Central mass of polycrystal α+ Neumann bands
		≈4·5	0·25	≈2·1	<0·02	Estimated average in zoned rim

Method

Samples were selected by hand from a magnetic fraction of soil 14162,80, which was collected as a bulk soil sample near to the lunar module. Four particles >1 mm in size were obtained. They were initially examined for surface features using both optical and scanning electron-microscope techniques. Subsequently they were individually mounted in plastic and polished for optical metallography and electron-microprobe analysis. Special attention was given to the compositions at the interfaces between phases and to concentration gradients within the metal. Bulk compositions were established by scanning the electron beam over an 80×100 μm area of a given sample.

Results and discussion

The sizes, bulk (microprobe) compositions, and metallographic structures of the four particles are recorded in Table I. It may be seen that all the particles lie in the conventional range of meteoritic Ni and Co contents proposed by Goldstein and Yakowitz (1971). The compositions in Table I also lie within the population ranges previously determined by Goldstein *et al.* (1972) for the smaller metal particles in the <1-mm soil fraction 14163,165 from the same bulk soil sample.

All of the metal particles in Table I have peripheral associations of silicate, which indicate that the metal had spent some time in the rocks of the lunar crust. It is therefore not to be expected that the original structure of any possible meteoritic projectile would be preserved in these particles. Indeed the structures and silicate associations of the first three particles are very similar to those reported by Goldstein *et al.* (1972) in the metal of the <1-mm soil fraction. Particle No. 7 has a unique and complicated structure and will be discussed separately.

Structural details for the four particles are reported and interpreted below.

Particle No. 3 is about 2 mm long and shaped like a boomerang. A few white glassy mineral grains are present at the surface. Fig. 1 shows the over-all microstructure of the sectioned and etched metal. The small, rare, crystalline silicates and sulphides at the periphery of this section indicate that the metal has been broken from a rocky matrix. The etched section also shows a narrow zone of surface damage such as might result from a rubbing or tumbling action on the particle. The deformed layer is partly recrystallized. Below the zone of surface damage the particle has a coarse polycrystalline α structure with no second phase. The metal is compositionally homogeneous at 5·4 wt. % Ni, 0·36 wt. % Co, and 0·17 wt. % P. The structure and composition of this particle are consistent with residence at about 500 °C, since, according to the Fe–Ni–P phase diagram, phosphide would precipitate below this temperature (Doan and Goldstein, 1970). The α grain boundaries show occasional thickening or migration, which could be due to reheating or the application of stress at about 500 °C. Neumann bands and shock structure, which formed at a later stage in the history of the particle, have also been subject to a mild reheating.

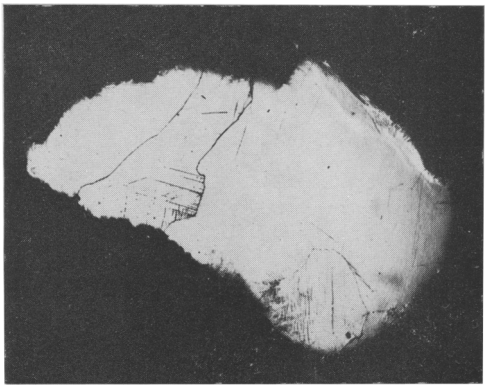

FIG. 1. Particle No. 3. Etched in Nital. Polycrystalline α-Fe showing local shock features and some surface deformation. Field of view 1·9 × 1·5 mm.

Thus in composition, structure, and silicate association this 2-mm particle is very similar to some of the 100 to 500-μm particles reported by Goldstein, Axon, and Yen (1972). It has 'meteoritic' proportions of nickel and cobalt but appears to have experienced a period of residence in the rocks of the lunar crust at a temperature of about 500 °C. It was broken out of the silicate host by a shock event and was subjected to surface abrasion in the regolith. At some stage subsequent to being liberated from the silicate it was mildly reheated.

Particle No. 4 is about 1·3 mm long. An etched microsection is shown in fig. 2*a* and the peripheral distribution of silicate is indicated in the S.E.M. fig. 2*b*. The peripheral silicate is a fragmented breccia, indicating that at one time the metal was embedded in a breccia rock. The metal is homogeneous in composition at 6·1 wt. % Ni, 0·55 wt. % Co, and 0·08 wt. % P. The metal has a complex reheated structure that

could be described as a polycrystalline array of α and a variety of α_2 showing variable grain size. The α contains a few fresh Neumann bands.

The composition, structure, and silicate association of this metal corresponds to some of the smaller particles previously reported for Apollo 14 soil. A possible history for this particle would be as follows: low-phosphorus metal of meteoritic nickel and cobalt content was embedded in a breccia rock. At some time, before, after, or probably during, the shock event that separated the metal from its breccia host, the metal

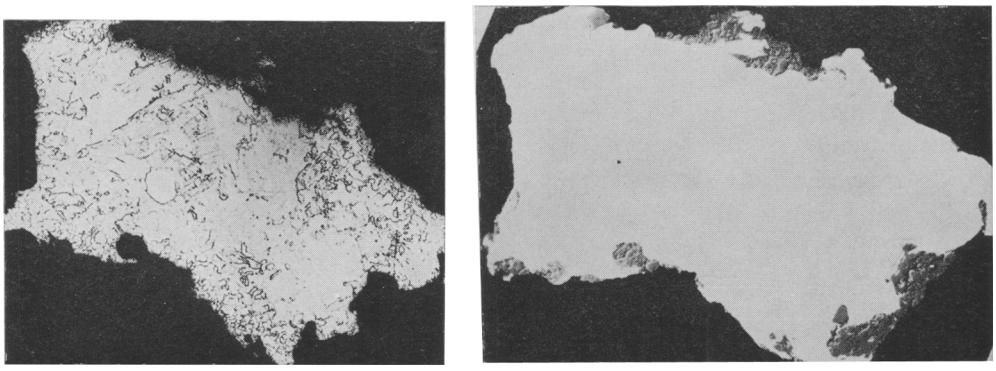

FIG. 2*a* (left): Particle No. 4. Etched in Nital. Reheated metal structure, α_2, α, variable grain size. Field of view 1·3×1·0 mm. *b* (right): Scanning electron microscope view of particle No. 4. showing the distribution of peripheral silicate material.

was heated into the γ range (>765 °C) and then rapidly cooled to produce the α_2 condition. It seems possible that a mild annealing treatment has subsequently operated and a final mild impact placed the Neumann bands in the specimen.

Particle No. 5 is about 2·6 mm long. It is a complex association of deformed metal and shock-generated glass. Globules of sulphide material are emplaced within some areas of the metal (fig. 3*a*) and smaller metallic globules are present in the glass (fig. 3*b*). As may be seen from fig. 3*a* some areas of metal are entirely free of sulphide globules. When the specimen is etched the α phase is found to be composed of small recrystallized grains, which are equiaxed and entirely lacking in directionality even in those regions where the sulphide inclusions are drawn out into well-developed slag lines as in fig. 3*b*. Bulk analyses (microprobe area scans) of the three types of metal (α free of sulphides; α+sulphide; small globules in glass) differ in sulphur content but are identical in nickel and cobalt at about 6·5 and 0·27 wt. % respectively. Representative analyses of the three types of metal are collected in Table I.

The compositional evidence, together with the juxtaposition of the three structures, suggests that a single shock event was responsible for redistributing the metal among the three types. Very similar structures are encountered in the larger shock-generated veins of chondritic meteorites. However, chondritic kamacite is usually richer in cobalt and the present particle is therefore likely to be a fragment of shock-generated target material from the lunar crust rather than a fragment from a chondritic projectile. This is also statistically more probable in view of the relative quantities of

projectile and target. However, the composition of the metal is such that it could have been part of a meteorite before it became embedded in the lunar crust.

Attention has been drawn to the over-all complexity of the structure. We visualize that it was formed in a shock event, the effect of which may be considered in three

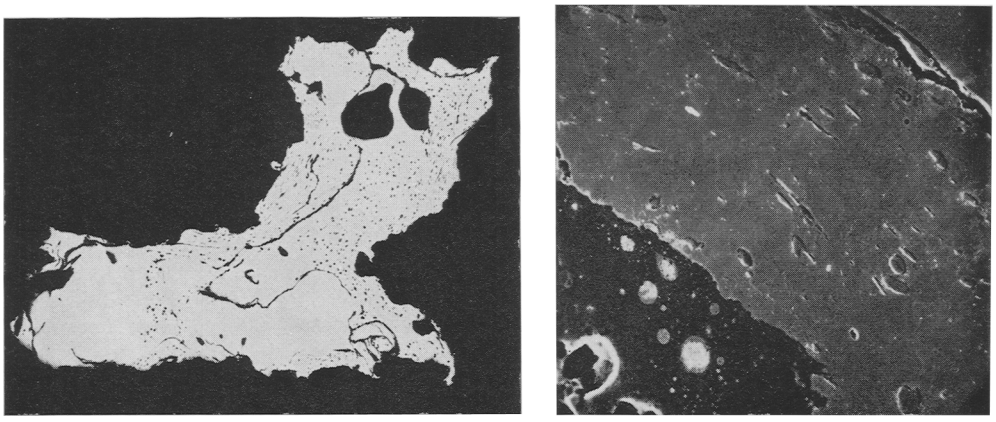

FIG. 3*a* (left): Particle No. 5. Unetched. Globules of sulphide in metal. Some metal areas are free of sulphide. The peripheral glass does not show in this mode of observation. See fig. 3*b*. Field of view 2·2 × 1·7 mm. *b* (right): Scanning electron-microscope picture of metal and peripheral glass at the edge of fig. 3*a*. The more extensive area is metal with deformed sulphide inclusions. The smaller, dark, area is glass with globular inclusions of metal–sulphide eutectic. Field of view 0·12 × 0·12 mm.

(overlapping) stages. Firstly there is the production of metal spheres in the glass, coupled with the emplacement of sulphide globules in the metal. Secondly there is gross plastic deformation, on a macroscopic scale, which manifests itself in the mixing together of metal and glass, in the elongation of sulphide particles, and in the production of fissures in the metal. These processes must have taken place while the material was hot, probably about 1000 °C. Thirdly, while the metal still retained its heat from the previous stages, there occurred an over-all recrystallization of the metallic matrix.

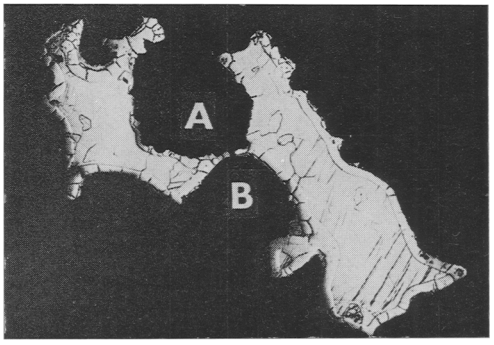

FIG. 4. Particle No. 7. Etched in Nital. The associated silicates are not shown in this mode of observation, see figs. 5*a*, 5*b*. A central mass of polycrystalline kamacite with a surrounding rim of compositionally zoned metal. Silicate is present at the metal interface in the major embayments A and B. Field of view 2·1 × 1·5 mm.

Particle No. 7 is about 2 mm long. The metal is of irregular shape and, as is shown by the etched section of fig. 4, there are two distinct zones of structure in the metal. Isolated fragments of minerals and glass are sporadically preserved along the exterior surface of the metal and the major embayments A and B in fig. 4 are occupied by the two different types of silicate material that are illustrated in figs. 5*a* and 5*b*, respectively.

For both metal and silicate material it is possible to identify 'older' and 'younger' structures and from their juxtaposition it seems possible that the older structures of both metal and silicate are of contemporaneous origin.

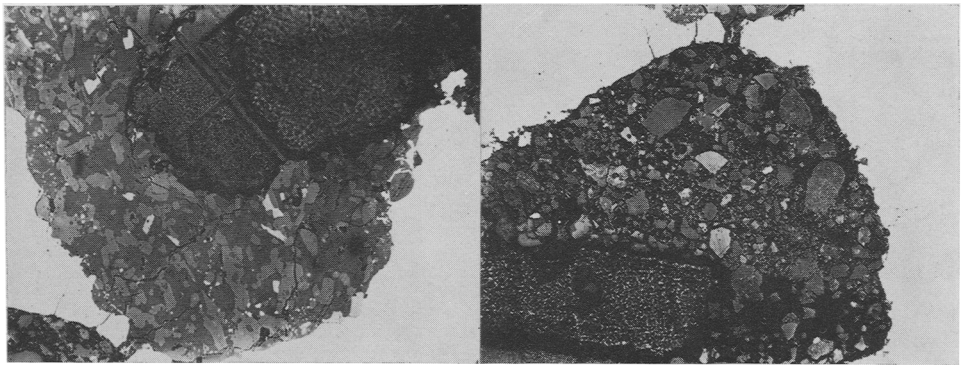

FIG. 5*a* (left): Crystalline rock, micronorite, at the metal interface of embayment A in fig. 4. The structureless dark area is mounting plastic burnt by exposure to the microprobe beam. Field of view 0·5×0·4 mm. *b* (right): Vitroclastic material at the metal interface of embayment B in fig. 4. The structureless dark area is mounting plastic burnt by exposure to the microprobe beam. Field of view 0·5×0·4 mm.

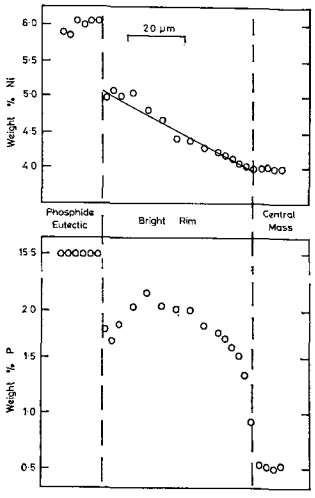

FIG. 6. Microprobe trace for Ni and P, showing the zoned distribution of these elements in the bright rim metal of fig. 4.

In the metal, fig. 4, the older structure is the large central mass of polycrystalline kamacite with occasional Neumann bands. The central metal region is entirely free of sulphide and phosphide inclusions. It is chemically homogeneous with 4·0 wt. % Ni, 0·25 wt. % Co, and 0·51 wt. % P in solid solution. According to the equilibrium diagram of Doan and Goldstein (1970) extensive precipitation of phosphide would be expected if a solid solution of this composition cooled slowly below *c.* 650 °C. Therefore we may conclude that the central mass of metal formed its structure above this temperature.

The younger metal structure is the bright rim of metal, approximately 50 μm wide, that almost (but *not* completely) surrounds the central mass. At one location, in embayment A, the central mass of metal comes into contact with the 'older' type of silicate material without the intervention of the bright rim of metal. The metal of the bright rim is a zoned solid solution in which the nickel and phosphorus contents take the form shown in the microprobe traces of fig. 6. The position of this microprobe trace is depicted in fig. 7, from which it may be seen that a typical metal–phosphide eutectic structure is present at the outer surface of the bright rim of metal. On detailed examination it appears that the eutectic is a ternary metal–sulphide–phosphide

association. The trace extends across the bright rim into the central mass of metal. The metal of the bright rim occasionally contains small particles of sulphide and phosphide and fig. 8 shows a rounded particle of sulphide lodged at the interface between the central mass of metal and the bright rim. Small (*c.*2–3 μm) particles of phosphide are observed at the interface between the bright rim and the central mass and also at kamacite grain boundaries within the bright rim. It is noteworthy that the

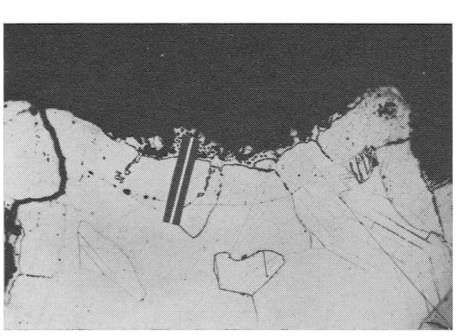

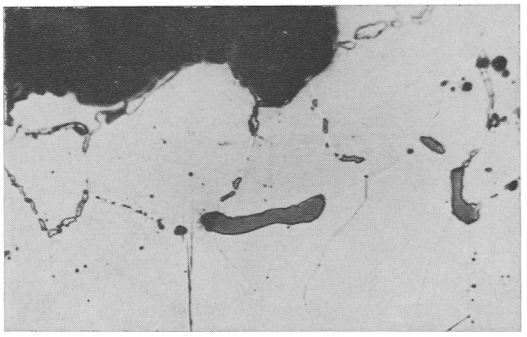

FIGS. 7 and 8: FIG. 7 (left). Location of microprobe trace across the compositionally zoned rim. Phosphide eutectic is present at the outer edge of the sample. Field of view 0·42 × 0·29 mm. The area shown in this figure lies in the smaller metallic area of Fig. 4 and is located parallel to and about one-third along the short side of Fig. 4. FIG. 8 (right). Large particles of sulphide (dark) at the interface between the central mass of metal and the bright rim. Small particles of phosphide (light) are present at kamacite grain boundaries within the bright rim. Field of view 0·2 × 0·13 mm.

grain boundaries within the bright rim are natural extensions of those within the central mass of metal. The observations so far reported for the bright rim suggest that a thin film of molten metal, rich in Ni and P, solidified epitaxially upon the central mass of solid metal to produce a layer of cored solid solution followed by a complex eutectic. In the absence of pressure effects the rim material would be liquid above about 1000 °C. Moreover, the liquid film must have formed and resolidified rapidly since the microprobe traces show a sharp discontinuity at the junction of the bright rim with the central mass. This discontinuity indicates that there was no measurable solid-phase diffusion of Ni or P from the liquid into the solid substrate. Additional information about the rate at which the rim material cooled may be obtained from the interface compositions of the metal and phosphide phases where they coexist at the outer edge of the bright rim. From the microprobe traces of fig. 6 values of 6·0 wt. % Ni and 15·5 wt. % P are obtained for the phosphide and 5·0 wt. % Ni with 1·75 wt. % P for the kamacite at the local interface. These interface compositions correspond to an equilibration temperature of 900 °C according to the Fe–Ni–P equilibrium diagram of Doan and Goldstein (1970). Microprobe traces are available at two additional locations on the sample and these give phosphide–metal interface values of 5·2 and 6·2 wt. % Ni in the phosphide, coexisting with 4·3 and 4·7 wt. % Ni and 1·6 and 1·5 wt. % P in the metal. These interface compositions indicate effective equilibration temperatures of 860 and 800 °C respectively. The high (800–900 °C) temperatures of effective equilibration again indicate that the bright rim material cooled rapidly.

The older silicate material, fig. 5*a*, is a fine-grained micronorite rock. Careful examination of the polished section by a combination of optical and microprobe methods shows that it is composed of crystals of hypersthene (*c.* 44 %) set in a matrix consisting of plagioclase (*c.* 35 %) and potash feldspar (*c.* 15 %) with armalcolite (*c.* 2 %), troilite (*c.* ½ %), and metallic nickel-iron (< ½ %) and there is about 3 % of whitlockite distributed as small crystals throughout the matrix. The Mg/(Mg+Fe) ratio of whitlockite within the matrix is high, 0·77–0·80 (analyses 71, 74, Appendix Table II). Embayment A, which is roughly circular and about 0·4 mm across, is almost completely filled with this micronorite. At the boundary between the metal and the micronorite there is a concentration of small (*c.* 50×20 μm) lenses of whitlockite producing a distinctly crenulate interface with the metal. This marginal whitlockite is in addition to the 3 % already reported within the matrix of the rock and has the lower Mg/(Mg+Fe) ratio of 0·53–0·69 (analyses 30, 42, Appendix Table II). The rare earths, Ce, Yt are below the limits of microprobe detection in both types of whitlockite.

Notes on the detailed petrology of the rock and analyses of its constituent minerals are recorded in the Appendix and Table II, together with the bulk composition of the micronorite (excluding the phosphate at the metal interface) and the C.I.P.W. norm calculated from the bulk analysis.

From the chemical and petrological examination it appears that the composition of the micronorite is similar to that of Fra Mauro deposits and its texture has affinities with the micro-breccia groundmass textures of groups 7 and 8 described by Warner (1972). Williams (1972) has suggested that rocks of this nature were held for 'short' periods at about 1100 °C, at which temperature they would be partially melted. Attention has already been drawn to the small area of contact between the micronorite and the homogeneous kamacite of the central mass. There is no solid phosphide at this interface but some sulphide is present. On either side of this interface a narrow finger of bright rim material has penetrated along the boundary between the central metal and the micronorite. The penetration of the bright rim material along the metal–silicate interface is suggestive of liquid penetration and this is supported by the observation that thin (<1 μm) veins of metal and troilite occupy grain boundary regions near the phosphide and penetrate in an irregular manner up to 150 μm along thermally produced cracks in the micronorite. It is clear that the micronorite in fig. 5*a* was present with the central mass of metal before the bright rim was formed.

The silicate material that fills the roughly hemispherical embayment about 0·35 mm across, fig. 5*b*, may be described as a weakly sintered, porous (*c.* 25 %), vitroclastic association of glass, devitrified glass, and mineral fragments. It is everywhere in contact with metal or eutectic of the bright rim. No whitlockite has been observed at the contact, which is cohesive but not welded. Detailed analytical and petrological data on this material is recorded in the Appendix and Tables III and IV. The vitroclastic material probably represents an impact-generated tuff into which the composite metal–micronorite fragment came to rest after a complex history of reheating, shock melting, and erosion. The limited number of analyses that have been made shows the relative concentration of glass types appropriate to the Apollo 14 site.

To recapitulate, the chemical and structural evidence suggests that the central mass of the metal particle once resided within a mass of micronorite. Apart from a small section that is preserved unchanged within embayment A, the original interface between the metal and its micronorite host has been almost completely replaced by zoned rim metal with its attendant eutectic phases. However, it is possible to suggest a plausible structure for the original micronorite–metal interface and to outline a sequence of events by which the particle developed its present structure.

To begin with, a kamacite particle of composition 4 wt. % Ni with $\frac{1}{2}$ to 1 wt. % P and of approximately the same shape and size as the metal of particle no. 7 was heated to a temperature of about 1100 to 1200 °C in contact with lunar silicate material. This allowed partial melting of the silicate material and total recrystallization while the metal remained unmelted. The silicate could have been a lunar surface soil that was locally heated by a nearby impact, but it is more probable that it was a relatively deep-seated part of the massive Fra Mauro fall-out or base-surge deposit within which the forces of thermal metamorphism are known to have operated. This process produces a structure where the metal particle is surrounded by a micronorite that was partially melted.

On cooling from 1200 °C the phosphorus in the homogeneous metal reacted with the silicate to produce whitlockite at the micronorite–metal interface. The rate of phosphorus diffusion falls with decreasing temperature and below about 1000 °C would become severely restricted in the solid micronorite. However, phosphorus diffusion remains possible within the metal phase and from a metal solid-solution containing 4 wt. % Ni and about 1 % P discrete precipitates of a phosphide phase would begin to exsolve at about 750 °C. The most favourable location for such phosphide precipitation to commence would be the metal–silicate interface. In our earlier studies of metal in the smaller size fractions we have encountered many examples of metal with phosphide (and sulphide) located along part of the metal–silicate interface (Goldstein and Axon, 1973). At 650 °C, according to the equilibrium diagram of Doan and Goldstein (1970), the phosphide, now concentrated as a peripheral rim to the homogeneous core of kamacite, would contain about 8 wt. % Ni. At this stage further cooling of the micronorite and its enclosed kamacite fragment with an almost complete schreibersite rim may have taken place but it has left no textural or chemical record. In particular, below 650 °C no further precipitation of phosphide occurred. This is inferred from the composition of the homogeneous core kamacite, 3·9 wt. % Ni, 0·51 wt. % P.

If, while at 650 °C, or some lower temperature, the material was involved in a shock event of sufficient intensity it could be altered into its present condition. Shock processes in phases of different compressibilities (phosphides, kamacite, silicate, sulphide, voids) give markedly different peak pressures and instantaneous temperatures. In the present case it is to be expected that higher temperatures were generated at the phosphide–(sulphide)–metal interfaces than within the bulk of the homogeneous kamacite. Therefore a shock that was capable of raising the metal–phosphide rim to the effective eutectic temperature would produce around the edge of the metal a film of molten liquid rich in nickel and phosphorus and containing also subordinate sulphide.

Cooling from the shock temperature was rapid and was accompanied by the epitaxial resolidification of a phosphorus- and nickel-rich zoned solid solution on to the solid metal of the homogeneous core. Some sulphide from the original interface became incorporated in the liquid film and was emplaced in the resolidified rim zone, both within the solid-solution region and within the metal–phosphide eutectic. The interface equilibria between metal and phosphide at the eutectic correspond to a temperature of ~850 °C, implying a rapid cooling process during the formation of the bright rim structure.

No relict ε-iron structure has been observed in the core kamacite. This suggests that the shock event took place in the rock at an initial temperature of about 650 °C while the original ejecta deposit was still cooling off. The pressure–temperature diagram for iron derived by Bundy (1965) shows that a shock event acting on homogeneous kamacite at this temperature would not produce the ε-iron transformation but would give recrystallized kamacite.

After the major shock event and production of the zoned rim the composite metal particle was involved in a further, mild, impact event, which removed the micronorite and much of the contact type of whitlockite from a large part of the bright rim. The partially stripped metal grain came to rest in a fine-grained vitroclastic deposit that was generated from the Fra Mauro formation of which the metal–phosphide–micronorite fragment was originally a part. The vitroclastic matrix was a surface or near-surface deposit as is shown by its high porosity. It is doubtful if its temperature on deposition exceeded 750 °C and cooling must have been extremely rapid since the deposit is weakly sintered and retains a high porosity, only a proportion of the constituent glass has devitrified, and no exsolution or reheating effects are present in the metal.

The final event or events that brought particle No. 7 and the others described in this paper into the surface regolith from which 14162,80 was collected are minor impacts. The shocks must have been weak since the fragment has not been reheated and its only manifestation is the development of Neumann bands in the kamacite.

REFERENCES

BLAU (P. J.), AXON (H. J.), and GOLDSTEIN (J. I.), 1973. *Journ. Geophys. Res.* **78**, 363–74.
BRETT (R.), 1965. *Amer. Min.* **52**, 721–33.
BUNDY (F. P.), 1965. *Amer. Journ. Appl. Phys.* **36**, 619.
DOAN (A. S., Jr.) and GOLDSTEIN (J. I.), 1970. *Met. Trans.* **1**, 1759–67.
GOLDSTEIN (J. I.) and AXON (H. J.), 1973. Supplement 4, *Geochimica Acta*, 1. 751–75. Pergamon Press.
—— —— and YEN (C. F.), 1972. Supplement 3, Ibid. 1. 1037–64, M.I.T. Press.
—— and YAKOWITZ (H.), 1971. Supplement 2, Ibid. 1. 177–91, M.I.T. Press.
KELLY (W. R.), HOLDSWORTH (E.), and MOORE (C. B.), 1974. *Geochimica Acta*, **38**, 533–43.
STATHAM (P. J.), 1976. *X-Ray spectroscopy*. In press.
WARNER (J. L.), 1972. Supplement 3, *Geochimica Acta*, 1. 623–43, M.I.T. Press.
WILLIAMS (R. J.), 1972. *Earth Planet. Sci. Lett.* **16**, 250–6.

[*Manuscript received 20 May 1975, revised 16 October 1975*]

APPENDIX

Petrographic description and analytical data on the micronorite (A) and vitroclastic (B) material associated with particle No. 7.

The micronorite may originally have been a fine-grained soil that was subsequently heated for a 'short' period to *c.* 1100 °C or it may have been a fine-grained ejecta or base-surge deposit in which the residual temperature approached 1100 °C for a 'short' period. Both situations would allow partial melting and extensive recrystallization of the silicates. The metal fragment (4 wt. % Ni 1 to ½ wt. % P) would not melt under these circumstances but the phosphorus in the metal would be available for reaction with the surrounding silicate to produce lenses of whitlockite at the metal–silicate interface. Analyses of this type of whitlockite are given in Table II, analyses 30, 42.

TABLE II. *14162,80; minerals of micronorite in embayment A of particle No. 7*

	27	41	28	28, 1	30	42	71	74	32	32A	34	AV
SiO_2	53·53	52·44	0·40	0·00	0·00	0·00	0·64	0·00	51·07	55·16	48·96	51·26
TiO_2	0·85	0·85	70·85	73·21	0·95	0·00	0·00	0·00	0·14	0·15	0·19	2·61
Al_2O_3	1·22	0·96	1·30	1·35	0·00	0·00	0·00	0·00	24·71	26·39	33·26	12·36
P_2O_5	0·00	0·00	1·23	0·00	46·51	45·69	47·39	47·72	1·94	0·00	0·00	0·69
Cr_2O_3	0·44	0·53	1·09	1·12	0·00	0·00	0·00	0·00	0·00	0·00	0·00	0·23
FeO	14·04	14·63	16·36	16·91	2·80	5·95	2·07	1·68	0·61	0·66	0·00	9·84
MnO	0·25	0·27	n.d.	0·00	0·00	0·00	0·00	0·00	0·00	0·00	0·00	0·15
MgO	27·26	27·25	7·16	7·40	3·45	3·76	4·09	3·69	0·17	0·18	0·00	11·45
CaO	1·87	1·13	1·23	0·00	45·63	44·12	45·94	46·88	12·38	10·88	16·02	6·90
Na_2O	0·00	0·00	0·00	0·00	0·00	0·00	0·00	0·00	1·87	2·02	2·16	0·88
K_2O	0·00	0·00	0·00	0·00	0·00	0·00	0·00	0·00	4·24	4·58	0·27	2·16
	0·00	0·00	0·00	0·00	0·00	0·00	0·00	0·00	0·00	0·00	0·00	1·00
Total	99·46	98·06	99·62	100·00	99·34	99·52	100·13	99·97	97·13	100·02	99·96	99·53
Unit formulae:												*C.I.P.W. norm*
Si	1·939	1·933		0·000	0·000	0·000	0·033	0·000		2·520	2·244	QZ 3·97
Ti	0·023	0·024		1·980	0·036	0·000	0·000	0·000		0·005	0·006	OR 12·76
Al	0·052	0·042		0·057	0·000	0·000	0·000	0·000		1·437	1·742	AB 7·45
P	0·000	0·000		0·000	2·016	2·002	2·020	2·044		0·000	0·000	AN 23·40
Cr	0·013	0·016		0·032	0·000	0·000	0·000	0·000		0·000	0·000	DI 5·10
Fe	0·425	0·451		0·509	0·120	0·257	0·088	0·071		0·025	0·000	HY 37·84
Mn	0·008	0·008		0·000	0·000	0·000	0·000	0·000		0·000	0·000	OL 0·00
Mg	1·472	1·498		0·397	0·263	0·290	0·308	0·278		0·013	0·000	CM 0·34
Ca	0·073	0·045		0·000	2·503	2·445	2·488	2·541		0·532	0·787	IL 4·95
Na	0·000	0·000		0·000	0·000	0·000	0·000	0·000		0·179	0·192	AP 1·63
K	0·000	0·000		0·000	0·000	0·000	0·000	0·000		0·267	0·016	PY 1·89
Ionic ratios												
Mg	74·7	75·1		43·4	68·7	52·9	77·8	79·7				
Fe	21·6	22·6		56·1	31·3	47·1	22·2	20·3				
Ca	3·7	2·3		—	—	—	—	—		54·4	79·1	
Na										27·3	19·3	
K										18·3	1·6	

27, 41 Hypersthene.
28 Armalcolite, 28, 1 Recalculated to 100 % after removal of SiO_2, CaO, P_2O_5.
30, 42 Whitlockite in embayments adjacent to schreibersite–Fe-metal eutectic or phosphorus-enriched metal.
71, 74 Whitlockite away from metal contact in micronoritic rock.
32 Feldspar-rich matrix between hypersthene crystals.
32A Analysis 32 recalculated to 100 % after deduction of CaO and P_2O_5 equivalent to whitlockite.
34 Plagioclase analysis normalized after removal of S as troilite.
AV Estimated bulk composition of melt rock in embayment A, excluding phosphate at immediate contact with metal.

All analyses performed with energy-dispersive electron-probe systems (Statham, 1976).

The micronorite is composed of crystals of hypersthene set in a matrix of plagioclase and potash feldspar with minor quantities of armalcolite, troilite, metal, and whitlockite.

Whitlockite within the mass of the micronorite occurs as hypidiomorphic crystals moulded on armalcolite or hypersthene but idiomorphic against feldspar. The crystals range in size from 3 to 25 μm. Analyses 71, 74 of Table II relate to this occurrence of whitlockite.

Hypersthene crystals are idiomorphic, from 10 to 50 μm in length and may include

micron-sized droplike crystals of plagioclase. In composition it is rather uniform around En75 Fs22 Wo3. Analyses 27, 41, Table II.

Armalcolite occurs in idiomorphic to hypidiomorphic tablets from 15 to 3 μm in size. It is often associated with small allotriomorphic crystals of whitlockite and minute interstitial areas, 1 μm in size, of troilite or Fe-Ni metal. An armalcolite analysis is given at 28 in Table II.

Plagioclase and potash feldspar occur interstitially and individual crystals were recognized

TABLE III. *14162,80; mineral-fragments associated with glass fragments of Table IV in the porous vitroclastic material filling embayment B of particle No. 7*

	04	14	24	02	20	06	03	13	11	28
SiO_2	37·54	54·35	52·73	49·04	53·53	49·96	46·34	47·02	49·22	45·70
TiO_2	0·00	0·44	0·92	0·48	0·69	1·63	0·00	0·12	0·00	0·12
Al_2O_3	0·00	0·00	0·79	0·27	1·77	2·68	32·91	33·13	32·43	34·44
Cr_2O_3	0·00	0·26	0·49	0·11	0·91	1·09	0·00	0·12	0·00	0·00
FeO	25·79	16·37	17·30	34·25	17·18	13·89	0·57	0·81	0·75	1·31
MnO	0·16	0·28	0·24	0·45	0·41	0·27	0·00	0·00	0·00	0·00
MgO	35·96	27·18	23·92	10·61	21·61	13·42	0·00	0·28	0·00	0·00
CaO	0·22	1·11	2·32	3·34	5·35	17·04	17·04	17·25	16·17	18·45
Na_2O	0·00	0·00	0·00	0·00	0·00	0·00	2·02	1·09	1·98	0·92
K_2O	0·00	0·00	0·00	0·00	0·00	0·00	0·00	0·14	0·09	0·00
P_2O_5	0·00	0·00	0·00	0·00	0·00	0·00	0·00	0·00	0·00	0·00
Total	99·67	99·98	98·71	98·55	101·45	99·98	98·88	99·96	100·64	100·94
Unit formulae:										
Si	0·997	1·973	1·957	1·991	1·947	1·891	2·161	2·166	2·241	2·098
Ti	0·000	0·012	0·026	0·015	0·019	0·046	0·000	0·004	0·000	0·004
Al	0·000	0·000	0·035	0·013	0·076	0·120	1·809	1·799	1·740	1·864
Cr	0·000	0·007	0·014	0·003	0·026	0·033	0·000	0·004	0·000	0·000
Fe	0·573	0·497	0·537	1·163	0·523	0·440	0·022	0·031	0·029	0·051
Mn	0·004	0·009	0·008	0·016	0·013	0·009	0·000	0·000	0·000	0·000
Mg	1·423	1·471	1·323	0·642	1·171	0·757	0·000	0·019	0·000	0·000
Ca	0·006	0·043	0·092	0·145	0·209	0·691	0·851	0·851	0·789	0·908
Na	0·000	0·000	0·000	0·000	0·000	0·000	0·182	0·097	0·175	0·082
K	0·000	0·000	0·000	0·000	0·000	0·000	0·000	0·008	0·005	0·000
P	0·000	0·000	0·000	0·000	0·000	0·000	0·000	0·000	0·000	0·000
Mg	71·3	73·2	67·8	32·9	61·5	40·1				
Fe	28·7	24·7	27·5	59·7	27·5	23·3				
Ca		2·1	4·7	7·4	11·0	36·6	82·4	89·0	81·4	91·7
Na							17·6	10·2	18·1	0·3
K							0·0	0·8	0·5	0·0

04, Olivine; 14, 24 Hypersthene; 02, 20 Pigeonite; 06 Augite; 03, 13, 11, 28 Plagioclase.

only with difficulty in reflected light in the polished mount. Their inferred occurrence as a rather fine-grained intergrowth is supported by the difficulty of obtaining a 'pure' analysis with the electron-probe. A typical plagioclase analysis is quoted as analysis 34 in Table II and a feldspar-rich matrix material and its composition recalculated after the deduction of whitlockite is quoted as analysis 32 and 32A in Table II.

The *vitroclastic material* in embayment B does not contain whitlockite. It is porous and weakly sintered. Vitric and mineral clasts in the size range 40 to 5 μm compose about 60 % of the rock and are set in a matrix of angular fragments < 5 μm in diameter. The larger clasts

are subrounded and the smaller tend to be subangular. Clasts of finely devitrified glass, in which a microcrystalline structure is visible in reflected light at × 500 magnification, compose about 35 % of the rock; they have a dark-grey reflectivity and predominate in the > 10-μm size range. Glass fragments that still retain their vitric state have a higher reflectivity; they appear pale grey, predominate in the > 10-μm size range and compose about 15 % of the rock. Mineral fragments compose about 10 % of the rock with plagioclase (or maskelynite) and hypersthene predominating over olivine and clinopyroxene. Representative analyses of minerals are quoted in Table III and of the glasses or their devitrified equivalents in Table IV.

TABLE IV. *14162,80 glass or devitrified glass fragments in porous vitroclastic material in embayment B of particle No. 7*

	26	10	21	09	01	23	22	05
SiO_2	42·72	50·50	50·50	49·56	45·90	48·55	43·88	44·27
TiO_2	4·00	2·93	2·27	1·48	0·84	1·88	0·32	0·20
Al_2O_3	13·10	14·50	14·76	16·02	17·06	17·46	23·88	25·25
Cr_2O_3	0·30	0·00	0·32	0·28	0·15	0·17	0·16	0·17
FeO	17·26	11·93	11·08	11·77	12·52	11·59	7·15	6·79
MnO	0·12	0·19	0·20	0·15	0·18	0·16	0·13	0·00
MgO	9·99	8·32	7·87	8·48	10·92	6·39	9·09	7·19
CaO	10·66	10·39	9·76	10·81	10·54	11·47	14·31	15·06
Na_2O	0·03	0·71	1·19	0·98	0·57	0·89	0·03	0·00
K_2O	0·25	0·29	0·74	0·36	0·20	0·59	0·00	0·00
P_2O_5	0·00	0·00	0·00	0·00	0·00	0·00	0·00	0·00
Total	98·43	99·76	98·69	99·89	98·88	99·15	98·95	99·16
C.I.P.W. norm wt %:								
QZ	—	6·12	3·88	1·25	—	1·90	—	—
OR	1·48	1·71	4·37	2·13	1·18	3·49	—	—
AB	0·25	6·01	10·07	8·29	4·82	7·53	0·25	—
AN	34·87	35·52	32·75	38·25	43·40	41·90	65·02	69·98
DI	14·91	13·18	12·90	12·68	7·30	14·47	4·85	4·68
HY	28·64	31·65	29·94	34·06	26·51	28·04	14·69	17·48
OL	10·25	—	—	—	13·85	—	13·29	7·32
CM	0·44	—	0·47	0·41	0·22	0·25	0·24	0·25
IL	7·60	5·56	4·31	2·81	1·60	3·57	0·61	0·38
EN in HY. Mol %	56·6	70·0	60·70	59·1	62·1	53·3	70·1	66·2

The trend of CaO against Al_2O_3 for the glasses has been plotted and is found to be similar to the trends observed at Apollo 14 and other sites. The limited number of analyses that have been made show the relative frequency of glass types appropriate to the Apollo 14 location. Fra Mauro basaltic glasses of the high and medium potassium types predominate along with Highland basalt glass. Anorthositic glass is rare and only one fragment of possible mare basalt glass was found.

Of the mineral analyses only the high albite content of the plagioclase is possibly characteristic of the Fra Mauro formation. The pyroxenes and olivines show no particular diagnostic features, even though they fall in the composition fields that Bence and Papike (1972) have delineated as characteristic of Apollo 14 basalts.